Contents lists available at ScienceDirect

European Polymer Journal

journal homepage: www.elsevier.com/locate/europolj

Osteogenic scaffolds based on fumaric/N-isopropylacrylamide copolymers: Designed, properties and biocompatibility studies

M. Leticia Bravi Costantino[a], M. Susana Cortizo[a], Ana M. Cortizo[b], Tamara G Oberti[a],*

[a] *Instituto de Investigaciones Fisicoquímicas Teóricas y Aplicadas (INIFTA), Facultad de Ciencias Exactas, Universidad Nacional de La Plata – CONICET CCT-La Plata, CC 16 Sucursal 4, 1900 La Plata, Argentina*
[b] *Laboratorio de Investigaciones en Osteopatías y Metabolismo Mineral (LIOMM), Departamento de Cs. Biológicas, Facultad de Cs. Exactas, UNLP, La Plata, Argentina*

ABSTRACT

In the present work the creation of a new biomaterial aimed at bone tissue regeneration is shown, covering the synthesis of the polymers, the material design and their exhaustive physicochemical and biological characterization. The copolymers of dioctyl fumarate (DOF) and N-isopropylacrylamide (NIPAM) were synthetized and characterized by size exclusion chromatography, ^{1}H NMR and its thermal properties were studied by DSC and TGA analyses. Based on their properties, two copolymers with different DOF content were selected as raw material to design scaffolds for bone tissue regeneration. The scaffolds were prepared by casting and electrospinning technique, giving rise to biomaterials with particular chemical and topographic surface which were characterized by water contact angle and scanning electron microscopy (SEM) analysis. The cytotoxicity and biodegradation by murine macrophage RAW 264.7 cells was assay, while biocompatibility and osteogenic induction were made using bone marrow progenitor cells (BMPC). None of the biomaterials obtained showed cytotoxicity. The biological properties suggest that the cells adhere and proliferate better on biomaterials with higher DOF content and fibrous morphology. All scaffolds support osteoblastic cell differentiation, but to a greater extent on the biomaterial that has higher DOF content prepared by casting. Altogether, our results suggesting that these biomaterials could be useful in the bone tissue engineering.

1. Introduction

The incidence of bone defects as a result of various diseases or accidents is a problem that affects the world population and increases with the age of people. Bone has a hierarchical and complex structure that supports its diverse mechanical, biological and chemical functions [1]. However, when the regeneration of large bone defects is not possible through self-repairing mechanisms, it is necessary to resort to other strategies. Thus, tissue engineering, based on a combination of scaffolds, cells and biofactors, has emerged as a novel and versatile tool for the restoration of various tissues, including bone tissue. The design of three-dimensional scaffolds with interconnected pore structures and appropriated surface properties is very important to guide cell adhesion and proliferation, as a first stage toward to specific cell differentiation which promotes the tissue regeneration. In addition, scaffolds addressed to bone tissue engineering must meet other important requiments such as those related to their surface and topographic characteristics, mechanical properties and osteogenic ability [2]. Despite the plethora of available biomaterials to treat bone defects, only a

small number has reached clinical use, this is the reason why new developments are still necessary [3].

Biomaterials employed in tissue regeneration have been developed using different types of natural or synthetic polymers, such as dextran, cellulose, gelatin, chitosan, alginate [4,5] or polyesters, acrylates and methacrylate [6,7]. Fumaric polymers can be considered competitive with methacrylics polymers because they exhibit similar physicochemical properties. In addition, fumaric monomers can be produced by fermentation processes from renewable resources which make them precursors of interest from the economic and environmental point of view. Homo and copolymers from dialkyl fumarates have been previously studied in our group as biomaterials directed towards various biomedical applications, such as scaffolds for bone tissue regenerations and membrane for transdermal delivery system (TDS). They were biodegradable by cellular mechanisms and were able to support osteoblastic growth without evidence of cytotoxicity [8,9]. In addition, the inclusion of nanohydroxyapatite in a compatibilized blend of poly(diisopropyl fumarate) (PDIPF) and poly(e-caprolactone) (PCL), significantly improves the cell biocompatibility and osteogenicity of the

scaffolds [10]. On the other hand, a borax cross-linked scaffold based on fumarate-vinyl acetate copolymer and chitosan demonstrate the versatility of this material for osteo- and chondrogenic development [11]. In another area of applications, we show that the appropriate selection of co-monomers allows designed a membrane with right properties for TDS system including a bisphosphonate [12,13].

Based on these previous developments, in this work an economic and novel biomaterial was designed using fumaric copolymers. In particular, dioctyl fumarate (DOF) and N-Isopropylacrylamide (NIPAM) monomers were selected to synthesize new copolymers with different compositions and polarity, due to that these characteristics have a significantly influence on cell biocompatibility. Furthermore, the biocompatibility and biodegradability of PNIPAM hydrogels were previously demonstrated [14]. Our copolymers were obtained in order to evaluate the influence of the macromolecular characteristics as well as the scaffold morphology on their biocompatibility and osteogenicity. In addition, the copolymerization behavior of this new system was analyzed for the purpose of understand the structure-properties relationship, as well as their thermal properties related to the conditions of processing and sterilization. With the intention to evaluate the cellular response over different surface topography of the scaffolds, films and fibrous matrices were designed. We hypothesize that the rational design of a scaffold for the best growth and development of osteoblasts is based on the combination of hydrophobic and hydrophilic monomers, which will allow reaching an adequate balance of polarity of biomaterial, together with an appropriate superficial morphology.

2. Experimental

2.1. Materials

Dioctyl fumarate (DOF) monomer was prepared and purified as previously described [12]. N-Isopropylacrylamide (NIPAM, 97%) was purchased from Sigma-Aldrich (Buenos Aires, Argentina), which was recrystallized from hexane. 2,2′-Azobisisobutyronitrile (AIBN) was purchased from Sigma-Aldrich (Buenos Aires, Argentina) and used after recrystallization from methanol. Dimethyl-2,2′-azobis(isobutyrate) (MAIB) was prepared in our laboratory following a previously published methodology [15]. Toluene, hexane, chloroform and other solvents were purchased from Cicarelli and Anedra (PA) (Buenos Aires, Argentina).

2.2. Copolymer synthesis

Radical copolymerization of DOF with NIPAM was carried out in toluene solution (25%) under thermal heating at 60 °C, following a published procedure [16]. Briefly, different amounts of both monomers and the solvent were introduced into a reaction tube together with the previously weighed mass of initiator (AIBN or MAIB, 40 mM). The mixtures were degassed by three freeze-pumpthaw cycles in a Schlenk line system, and then the tube was sealed and immersed into a thermostat at 60 °C. The reaction time was of 4 d in the absence of light. After reaching room temperature, the copolymers were isolated by hexane addition and purified twice by solubilization–precipitation (chloroform:hexane, 1:10). Finally, the copolymers were dried at constant weight for conversion (%C) estimation by gravimetry. The copolymers were designated DFN.

2.3. Copolymer characterization

^{1}H NMR spectra of DFN were recorded with a Bruker-500 MHz (Avance-AV 500) at 35 °C in deuterated chloroform (DCl$_3$). Tetramethylsilane (TMS) was used as an internal standard.

A Shimadzu IR-435 spectrometer was used to record the infrared spectra of copolymers as a capillary film onto a sodium chloride (NaCl) window, between 4000 and 400 cm^{-1} with a resolution of 4 cm^{-1} and

32 accumulated scans. The EZOMNIC software (EZOMNIC 7.4.127, Thermo Fisher Scientific Inc, Madison, WI, USA) was used to analyze the spectra.

The molecular weight distribution and the average molecular weights were determined by size exclusion chromatography (SEC), using a LKB-2249 instrument at 25 °C. A series of four μ-Styragel ® columns, ranging in pore size 10^5, 10^4, 10^3, 100 Å, was used with chloroform as an eluent. The sample concentration was 4–5 mg/mL and the flow rate was 0.5 mL/min. The polymer was detected by the carbonylic absorption of the ester group (5.75 μm), using an infrared detector (Miram 1A Infrared Analyzer) and the calibration was done with poly(methyl methacrylate)(PMMA) standards supplied by Polymer Laboratories and Polysciences.

Thermogravimetry analysis (TGA) was performed in a TGA-51 Shimadzu thermogravimetric analyzer. Samples of 2–5 mg were heated from room temperature to 600 °C a heating rate of 10 °C/min under nitrogen flux (40 mL/min).

Glass transition temperatures (Tg) were measured employing a scanning calorimeter (DSC, Q2000-TA Instruments). The samples were scanned at 10 °C/min, from −50 to 200 °C, under dry nitrogen. Three consecutive scans were performed for each sample: heating/cooling/heating.

2.4. Scaffolds preparation

In order to perform experiments with macrophage cells in culture, and analyzed the effect of the surface topography, scaffolds of selected copolymers were obtained by two different methodologies: solvent casting and electrospinning. In the first case, polymer solution was prepared in chloroform (5%) and the solvent evaporated at room temperature on Teflon molds and then dried under vacuum until constant weight. These samples were designated as DFNXc, where X indicates the content of dioctyl fumarate monomer in the copolymer.

In the second case, electrospinning technique allows obtain fibrous scaffolds. For that copolymer solutions in chloroform (5%) were prepared. The solution was loaded into a standard 2.0 mL plastic syringe connected to a polyamide tube, the open end of which was attached to a blunt 21-Gauge stainless steel hypodermic needle (I.D. = 0.71 mm) used as the nozzle and a needle-to-collector distance of 10 cm. The flow rate was controlled by a programmable syringe infusion pump (ADOX Activa A22 S.A., Argentina) connected to the syringe. A high-voltage power source (MP SRL, High Voltage Power Source.) was used to charge the solution by attaching the electrode of positive polarity to the nozzle, and the grounding one to the aluminium collecting. Solutions were electrospinned at a positive high voltage gradient of 12 kV and a solution flow rate of 2.0 mL/h. The scaffolds thus obtained were dried under vacuum at room temperature to fully eliminate the residual solvent, and stored in a desiccator until use. These samples were designated as DFNXe, where X indicates the content of dioctyl fumarate monomer in the copolymer.

Both kinds of scaffolds were sterilized by UV exposition for 2 h [10] for biological assays.

2.5. Scaffolds characterization

Morphologies of surfaces scaffolds were qualitatively characterized by scanning electron microscopy (SEM). Samples were viewed under Philips 505 scanning electron microscope operated at an accelerating voltage of 20 kV. Polymeric surfaces were sputter coated with gold before viewing under SEM. The images were analyzed by using Soft Imaging System ADDA II.

The wettability of the scaffolds was analyzed by Water contact angle (WCA). The measurements were carried out using deionized water at room temperature, as previously published [8].

The thickness of the scaffolds was measured at several points using a micrometer (Black Jack, 0–25 mm ± 0.01) and the mean values were

calculated.

2.6. Cell culture and incubations

Murine macrophage RAW 264.7 cells were grown in DMEM (Invitrogen, Buenos Aires, Argentina) containing 10% fetal bovine serum (FBS, Natacor, Argentina), 100 U/mL penicillin and 100 mg/mL streptomycin at 37 °C in a 5% CO_2 atmosphere. For the experiments, scaffolds were cut to size, inserted in a 24-well plate and macrophages plated on them. These cells were used to evaluated the degradation of scaffolds as wells as the possible cytotoxicity. For the last assays, NO and cell counting were assessed according to our previous publication [16].

For biocompatibility assays bone marrow progenitor cells (BMPC) were used. BMPC were isolated from the femora of Sprague-Dawley rats and cultured according to Molinuevo et al. [17]. Cells were maintained in basal media (DMEM-10% FBS) at 37 °C. Biocompatibility was assessed by cell morphology (SEM and fluorescence microscopy), adhesion, proliferation and osteoblastic differentiation. All experiments with animals were done in conformity with the Guidelines on Handling and Training of Laboratory Animals published by the Universities Federation for Animals Welfare [18]. Approval for animal studies was obtained from our institutional animal welfare committee (CICUAL-FEC-UNLP Protocol Number 001-05-15).

2.7. In vitro degradation assay

To evaluate the possible degradation, the scaffolds were weighted (W_o) and incubated with RAW 264.7 macrophages in DMEM/10% FBS for 7 and 14 d. After that period cells were lysed with 0.1% Triton X-100, the scaffolds were washed several times with distilled water and dried until constant weight. After that the scaffolds were weighed again (W_t). Degradation was calculated as the weight loss of each scaffold during the culture period using the following expression:

$$\%Degradation = \frac{W_0 - W_t}{W_0}100 \qquad (1)$$

2.8. Cell morphology, adhesion and proliferation

The morphology of BMPC growing on different scaffold was evaluated by SEM, as described previously [19]. Briefly, cells were plated on films or fibers matrices during 24 h, samples were washed with PBS, fixed with 96% ethanol for 10 min at room temperature. After that, samples were dehydrated with graded ethanol series and finally dried at room temperature and coated with gold. The samples were analyzed as described for matrix alone.

In addition, the shape of BMPC and their interaction with the scaffolds was evaluated by fluorescence microscopy. For F-actin staining, after 2 h or 24 h in culture, cells were washed twice with PBS, fixed with 4% paraformaldehyde/PBS for 10 min at room temperature and permeabilized with 100% EtOH for 4 min at –20 °C. Alexa Fluor 488 Phalloidin stock solution in methanol (495/518 nm Life technology) was diluted in PBS (1:100) and incubated for 1 h at room temperatures in the dark, to stain F-actin fibers. Nuclei were visualized by Hoechst 33,258 counterstaining for 5 min (338/505 nm, Sigma-Aldrich). Samples were examined by a fluorescence microscopy equipped with appropriate filter sets, connected to a digital color camera (Olympus, Tokyo, Japan). The photographs were taken with an objective of 40X. Images were recorded with the cell Sens Software (Olympus, Tokyo, Japan) and were analyzed with the free software ImageJ.

The adhesion and proliferation of BMPC was evaluated by the 3-(4,5-dimethylthiazol-2-yl)-2,5-diphenyl tetrazolium bromide (MTT) assay. This assay measures the reduction of the tetrazolium salt MTT to formazan by intact mitochondria in living cells. Thus, absorbance change is directly proportional to the number of viable cells. Briefly, 2.5×10^4 cells per well in basal media were plated onto the scaffolds which were casted on multiwell culture plates and cultured during different periods of time: 2 and 4 h for adhesion, or 24 and 48 h for proliferation. After these culture periods, cells were incubated for two additional hours with a solution of 0.1 mg/mL MTT. After washing, the formazan precipitate was dissolved in dimethyl sulfoxide (DMSO) and the absorbance read at 570 nm.

2.9. Osteoblastic differentiation

Osteogenic induction of BMPC growing on scaffolds or tissue culture plate (TCP) was performed by incubating the cells in basal DMEM/10% FBS media (Basal condition) or in a media supplemented with β-glycerol-phosphate and ascorbic acid (Differentiation media) during different periods of time as previously reported [17]. After 15 d, the ability of the cells to express markers of osteoblastic phenotype associated with bone-forming capacity was evaluated by measurement alkaline phosphatase (ALP) activity following the methodologies previously described [9]. Briefly, measurement of ALP was carried out by spectrophotometric determination of initial rates of hydrolysis of p-nitrophenyl-phosphate (p-NPP) to p-nitrophenol (p-NP) at 37 °C for 10 min. p-NP was determined by absorbance at 405 nm. After 21 d, mineral deposits in the extracellular matrix were analyzed with the colorimetric assays of Alizarin S red [20].

2.10. Statistical analysis

Results are expressed as mean ± SEM and represent at least three different experiments performed in triplicate. Differences between the groups were assessed by one-way analysis of variance (ANOVA) using the Tukey post hoc test. For no normally distributed data, the non-parametric Kruskal-Wallis test with Dunn *post hoc* test was performed using GraphPad In Stat version 3.00 (Graph Pad Software, San Diego, CA, USA). $p < 0.05$ was considered significant for all statistical analyses.

3. Results and discussion

3.1. Copolymers synthesis and characterization

In this study, we prepared new amphiphilic fumaric copolymers by radical polymerization using two different of initiators (AIBN and MAIB) in order to evaluate its influence on the macromolecular characteristics. The structure of the copolymers obtained was identified by spectroscopic methods. FTIR (thin film, cm^{-1}): 3430 (N–H), 2982, 2930 (C–H), 1723 (C=O ester), 1646 (C=O amide), 1230, 1165(CO–OR), 1108 (C–O). Fig. 1 shows the structure and ^{1}H NMR spectrum of a representative sample. ^{1}H NMR (DCl$_3$C, δ_H, ppm): 0.90 (CH$_3$–CH$_2$–); 1.16 (CH$_3$–CH <); 1.29 (–(CH$_2$)$_4$); 1.45 (–CH$_2$–CH–O –); 1.64 (–CH$_2$– main chain); 2.18 (–CH–CON– main chain); 2.06–3.10 (–CH–COO– main chain); 4.03 (NCH <); 4.84 (–OCH <) and 6.35 (NH).

The composition of copolymers was estimated from the integral ratio of peaks at 4.84 and 4.03 ppm corresponding to (–OCH <) of DOF and (–NCH <) of NIPAM, respectively, using eq. (2).

$$F_1 = \frac{I(OCH)}{I(OCH) + 2I(NCH)} \qquad (2)$$

where F_1 is the mole fraction of DOF in the copolymer and I(OCH) and I(NCH) represent the ^{1}H NMR resonance peak areas at 4.84 and 4.03 ppm, respectively.

Table 1 summarizes the mole fraction of DOF in the feed (f_1), in the copolymer (F_1), percentage of reaction conversion (%C) and properties of the copolymers obtained. As can be see, different behavior was observed by the use of AIBN or MAIB as initiators, at same initiator
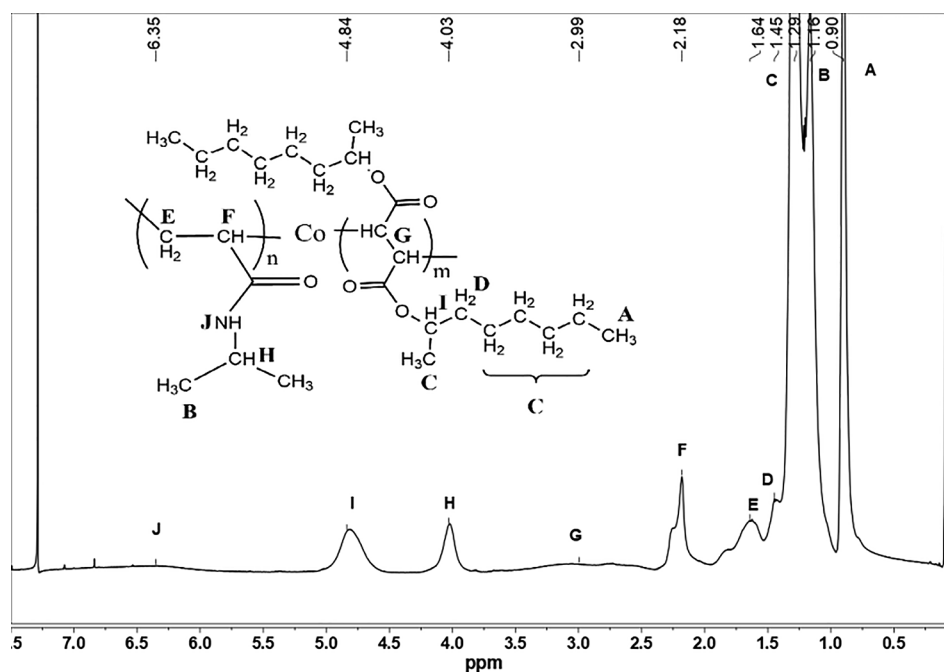
Fig. 1. ^{1}H NMR spectrum of DFN in CDCl$_3$ at 35 °C.

Table 1
Characteristics of the synthesized copolymers.

Sample	Initiator	f_1*	F_1*	%C	M_w (Kg/mol)	PDI
1	AIBN	0.30	0.10	26	–	–
2		0.50	0.10	14	11.62	2.36
3		0.60	0.59	13	17.08	2.80
4		0.70	0.71	10	15.04	2.84
5	MAIB	0.40	0.15	33	119.70	2.30
6		0.45	0.28	38	64.43	7.47
7		0.50	0.62	28	60.77	9.40
8		0.60	0.76	26	24.95	4.22

Reaction conditions: [Initiator] = 40 mM, [Monomers] = 75% toluene solution, 96 h at 60 °C.

* f_1 and F_1 are the mole fraction of DOF in the feed and in the copolymer, respectively.

concentration. In the first case, the conversion decreased when f_1 increase, while the %C was not affected significantly when MAIB was employed as initiator. These observations could be attributed to higher polymerization rate (Rp) of fumaric monomer in presence of MAIB, contrary to that observed for other vinyl or acrylic monomers, whose polymerization rate were independent of the nature of the initiator, as was previously demonstrated [21]. Some differences in average molecular weight (M_w) were also observed, when one and the other initiator were used. It is possible to see that when f_1 increased both M_w and the polydispersity index (PDI) almost do no change when AIBN was used as initiator. On the other hand, an increase of M_w and PDI was observed using MAIB as initiator in comparison with the M_w and PDI values determined employing AIBN initiator, under the same experimental conditions. This behavior could be attributed to the lower reactivity of the DOF with respect to NIPAM, which is highlighted in the presence of MAIB. In fact, with the same value f_1, a higher DOF content in the copolymer was found when MAIB was used as initiator. On the other hand, the high PDI observed could be a consequence of chain transfer reactions which broaden the molecular weight distribution, as was previously reported for similar systems [12]. In order to verify this hypothesis, the kinetic of a reaction initiated by MAIB ($f_1 = 0.5$) was carried out and the molecular weight distribution was monitored up to 4 d. Fig. 2 shows the chromatographic profiles corresponding to the
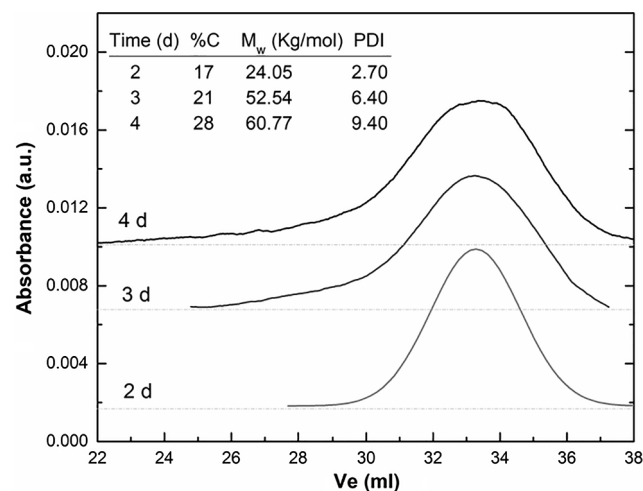

Fig. 2. Chromatographic profile of DFN60 (sample 7, Table 1) in function of time. Table insert presents the corresponding of reaction conversion, weight average molecular weight and polydispersity index.

samples obtained at 2, 3 and 4 d, while the value of reaction conversion, M_w and PDI were insert in the graph. It is possible to see an increase of the PDI when the conversion increased, which could be due to an increase in chain transfer reactions.

3.2. Structural analysis of DFN copolymers

Fig. 3 shows the plot of DOF mole fractions in the feed (f_1) versus the mole fraction of DOF in the copolymer (F_1) for the copolymers synthesized using the two initiators (AIBN and MAIB). In both cases the system shows the same tendency with greater variations in F_1 when $f_1 > 0.5$ which evinces the preference of the growing macroradical to incorporate DOF monomer. This result suggests higher reactivity of used acrylamide monomer, similar to that found for others copolymerizations of fumaric esters with acrylic monomers [21–23].

The different behavior observed, related with the kind of the initiator used could be attributed to that the primary radical generated
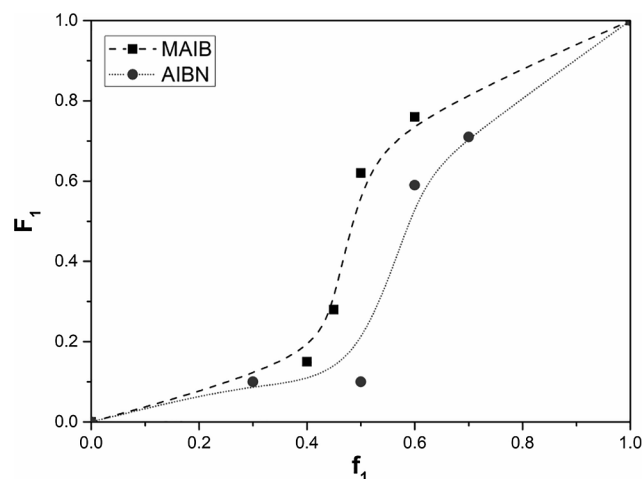
Fig. 3. Copolymer composition plot for DOF-NIPAM system. [Initiator] = 40 mM, 96 h at 60 °C. The lines are the eye guide.

from AIBN has lower initiation reactivity than that from MAIB, as was previously demonstrated for dialkyl fumarate homopolymerizations [24], which could lead to differences in the microstructure of the copolymers.

3.3. Thermal properties

Some of previously synthesized copolymers will be used as raw material to design scaffolds for bone tissue regeneration. Due to biomaterials addressed to these applications must be sterilized before to carried out biological assays, is important to know its thermal behavior to avoid its decomposition during sterilized process. Thus, the DSC of the copolymers synthesized was analyzed in order to obtain their glass transition temperature (Tg) value. Fig. 4 presents the corresponding thermograms together with the experimental Tg values for each sample (the numbers on the right correspond to the designation of each sample in Table 1). All copolymers shows a single Tg, which depends on the molar content of comonomers and presents an intermediate Tg value between those of the respective homopolymers, as expected for random copolymers. The previously reported Tg value for PNIPAM and PDOF are 135 °C and −14 °C, respectively [25,12]. As can be seen in Fig. 4, as the DOF monomer content in the copolymer increases, the Tg value decreases, both using AIBN and MAIB initiators (Fig. 4A and B). The Tg values for PDOF and for the copolymer with the highest DOF content

were not evident of thermograms, similar to what was previously observed by other researchers [26,27].

Based on the previously determined properties, samples 2 and 6 from Table 1 (designated as DFN10 and DFN30, respectively) were selected in order to analyze the effect of copolymer composition on the thermal stability by thermogravimetric analysis. The selection of analyzed polymers was based on some of its characteristics such as F_1 (comonomer composition in copolymer), M_w (average molecular weight), %C (conversion reaction) and Tg value, in order to design the best scaffold according its final physicochemical and biological properties.

Their decomposition curves are presented in the Fig. 5, from which the following parameters were obtained (Table 2): initial decomposition temperatures (IDT) and maximum decomposition temperatures (T_{max1} and T_{max2}).

The observed thermal events up to 200 °C in thermograms could be attributed to residual solvents or absorbed environmental water. Both copolymers seemed to decompose in a two-stage process and showed lower initial decomposition temperatures than PNIPAM homopolymer (350 °C). Silva and coll. reported that the thermal degradation of PNIPAM occurs in a single stage, close to 420 °C [25]. Previously was demonstrated that fumaric copolymers can decompose in one or two stages depending of the pair of comonomers and the first decomposition event can be attributed to the loss of the lateral group by cleavage reaction of the pendent group [22,28]. In the present case, the two thermal events observed can be awarded to loss of the dioctyl lateral group of fumarate monomer and to the final scission of main chain, respectively.

These results show that the synthesized copolymers exhibited high thermal stability which suggest that they could be subjected to a thermal sterilization process up to 100 °C without undergoing deformation or decomposition.

3.4. Scaffold characterization

Several studies have shown that surface chemistry and topographic characteristics (roughness, porosity and nanostructure) plays a large role not only in the initial cell adhesion, but also in the proliferation and differentiation of many cell types [29–31]. Therefore, we examined the morphological characteristics of scaffolds from samples 2 and 6 (See Table 1), prepared by casting and electrospinning, through SEM images (Fig. 6). These samples were labeled based on the comonomer composition, as was before indicated, (10 and 30 for samples 2 and 6, respectively) and the methodology used for its preparation (c and e, for
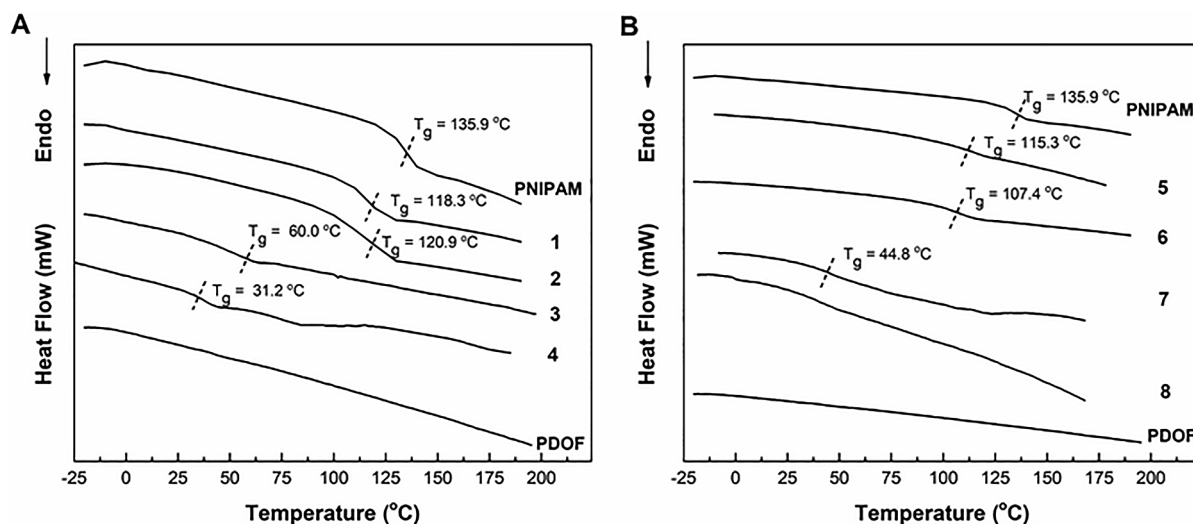

Fig. 4. DSC thermograms and Tg values of copolymers obtained: (A) samples 1–4 and (B) samples 5–8 from Table 1.
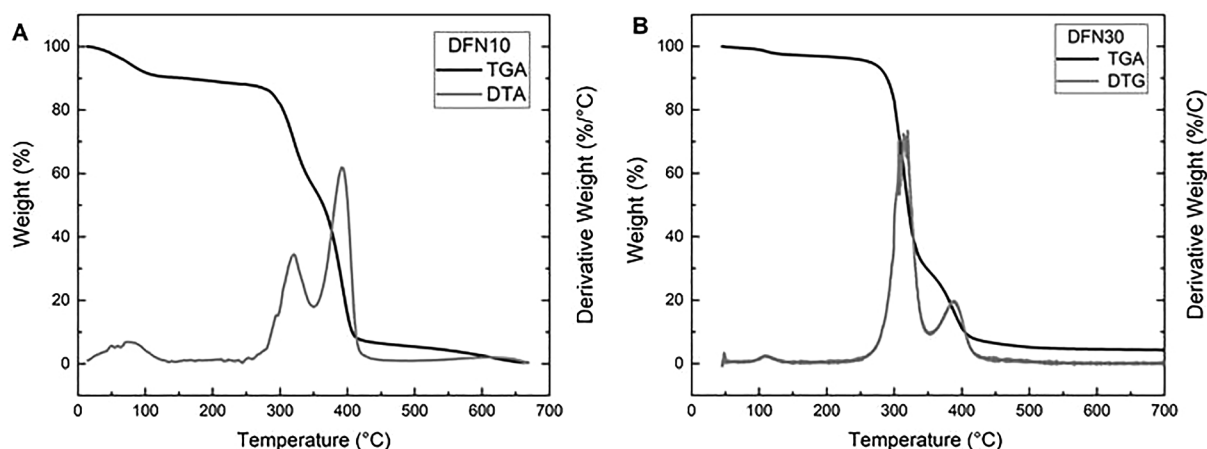
Fig. 5. TGA (black) and DTG (gray) curves under nitrogen atmosphere at heating rate of 10 °C/min for: (A) DFN10 and (B) DFN30.

Table 2
DSC and TGA data of selected copolymers.

Sample	F_1	T_g (°C)	IDT	T_{max1}*	T_{max2}*
DFN10	0.10	120.9	268	320 (33)	392 (49)
DFN30	0.28	107.4	254	315 (67)	382 (21)

Value in parentheses indicates the total mass loss (%) up to the stated temperature.

casting or electrospinning, respectively): DFN10c, DFN10e, DFN30c and DFN30e. The thickness of the scaffolds prepared by casting were 206 ± 6 μm and 230 ± 5 μm for DFN10c and DFN30c, respectively; while that for DFN10e and DFN30e, prepared by electrospinning technique the thickness were 72 ± 7 μm and 78 ± 2 μm, respectively.

Fig. 6(A) and (B) shows the micrographs of the surface morphology of solution-cast films of DFN10c and DFN30c, respectively. The images reveal smooth and homogeneous surfaces without porous and somewhat rough in the case of DFN10c. On the other hand, electrospinning methodology allows us to obtain 3D fibrous scaffolds, as can be seen in the SEM images (Fig. 6(C) and (D)). The micrographs show highly porous scaffold consisting of random fibers with diameters of 3.15 ± 0.30 μm and 2.92 ± 0.30 μm for DFN10e and DFN30e, respectively.

Besides, the initial cell-surface interaction is also depending of the hydrophilicity of the materials [32,33], due to biomaterial-cell interactions can be related to the wetting properties of the scaffold, thus influencing cellular behavior. In order to evaluate this important aspect, the water contact angle (WCA) of the membranes was analyzed in the present study. Fig. 7 shows the WCA of different scaffold previously mentioned, including the values corresponding to the membranes prepared from the homopolymers (PNIPAM and PDOF). It is possible to see an increase of the WCA with the increase of percentage of more hydrophobic monomer in the copolymer (DFN10 versus DFN30), which is more significant in the case of the scaffolds with fiber morphology. This
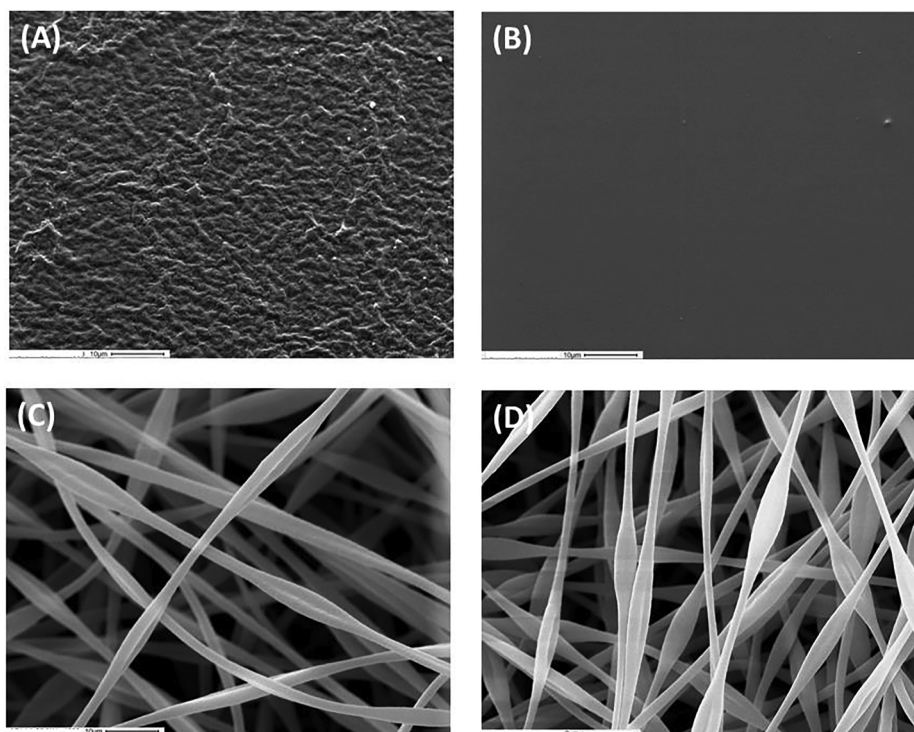

Fig. 6. Scanning electron micrographs showing the surface morphology of scaffolds: (A) and (B) solution-cast films of DFN10c and DFN30c, respectively; (C) and (D) fibrous scaffolds formed by electrospinning of DFN10e and DFN30e, respectively. Magnification 1000×.

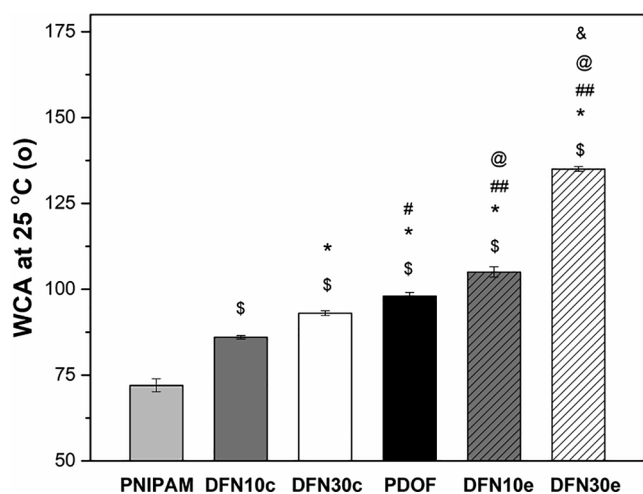**Fig. 7.** Water contact angle (WCA) of DFN scaffolds at room temperature. Data are expressed as mean ± SEM, n = 6. Differences are $ $p < 0.001$ vs PNIPAM; * $p < 0.001$ vs DFN10c; # $p < 0.05$, ## $p < 0.001$ vs DFN30c; @ $p < 0.001$ vs PDOF; & $p < 0.001$ vs DFN10e.

Fig. 8. In vitro degradation assay. Macrophage RAW 264.7 cells were cultured on the scaffolds during different periods of time and then evaluated the loss of weight. Data are expressed as mean ± SEM, n = 3. Differences were: * $p < 0.01$; ** $p < 0.001$ vs DFN10c and # $p < 0.01$; ## $p < 0.001$ vs DFN30c.

result is in agreement to expected, based not only on the copolymers composition but also on its morphology, as can be appreciate by the significant increase of this properties in the case of the fibers (DFN10e and DFN30e) in comparison to the casted scaffolds (DFN10c and DFN30c). This behavior could be explained based on different models which considered the effect of wetting of solids with porous or textured architecture [34,35]. In our samples, prepared by electrospinning, due to air pockets exist below the water droplet, the surface follows the Cassie-Baxter state model, which leads to an increase in the contact angle. Similar results were found for other systems based on the same materials but with different surface topography [30,36,37].

3.5. Degradation by macrophages

It is known that polyfumates have a skeleton composed of a linear structure of C—C which makes them have a lower biodegradability than other synthetic polymers. However, we previously demonstrated that they could be biodegradable by cellular mechanisms [8]. Thus, the possible degradation of the scaffolds was evaluated under cells conditions using RAW 264.7 macrophages at 37 °C and determining the weight loss after that 7 and 14 d. We found a linear increase in the weight loss for all scaffolds in function of the time (Fig. 8), with a maximum of about 11% and 15% of weight loss after 14 d of incubation for DFN10c and DFN30c respectively. In contrast, for DFN10e and DFN30e the corresponding values were around 4% and 6%, respectively. Thus, the degradation induced by macrophages was significantly lower ($p < 0.001$) for the scaffolds prepared by electrospinning than for those obtained by casting.

Under this degradation conditions we would made a projection of the scaffolds degradation at long time and to predict that the casted scaffolds will be completely degraded after 3–4 months, while that the fibrous scaffolds will be degraded after 8–12 months. These times are according to the bone regeneration in cases such as long bone fracture (3–9 moths) or cranio-maxillofacial applications (6–9 moths) [38,39]. With this result in mind, it could be possible to develop a scaffold with composition and morphology such that its degradation time to be similar to the regeneration of the host tissue.

3.6. Citotoxicity

The studies of NO and cell counting performed to evaluated the possible cytotoxicity of fibrous scaffold on macrophages, demonstrated no effects on these cells (data not shown). These results were similar to
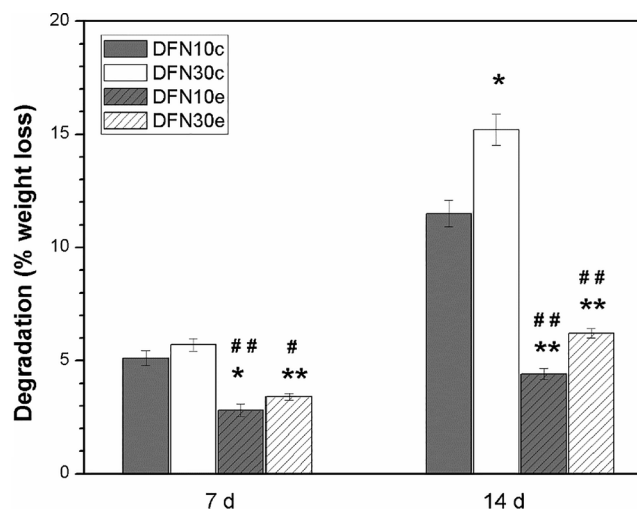
the reported for the film scaffolds in our previous publication [16], suggesting that neither the composition nor the topography induced toxic effects on the Raw 264.7 cells.

3.7. Biocompatibility studies

The biocompatibility of different scaffold was evaluated though the interaction with BMPC, assessing the cell viability, the actin- cytoskeleton development and the cell morphology by SEM.

The adhesion of BMPC to different scaffold was tested after 2 or 4 h and the proliferation after 24 and 48 h of culture, using the MTT assay (Fig. 9). It can be seen that cells attach and growth progressively until 48 h. However, the electrospun-like scaffolds (DFN10e and DFN30e) significantly promoted better cell attachment and proliferation, as compared to plane casted-matrix (DFN10c and 30c) at all-time point studied. It can be seen that cells adhere and growth almost equally to the 10c and 30c scaffold (Fig. 9A and B). However, the effect of the copolymer composition was evident in the fiber matrix's, with a significant increment of adhesion and proliferation when cells were cultured on the DFN30e scaffold. Altogether, the results suggest that both the surface topography and the copolymer composition can modulate the growth of the cells.

Fig. 9 also shows cells cultured for 2 h (Fig. 9C) or 24 h (Fig. 9D) on different scaffolds. It can be seen that initially cells maintain the rounded form with few extensions interacting with the scaffolds. According to the data of Fig. 9A, few cells were observed on the DFN10c and 30c matrix, in comparison with cells adhered to the fibrous scaffolds. After 24 h of culture, cells developed extensions and processes interacting with the matrix. More flattened and elongated cells were observed, with prominent stress fibres of the actin cytoskeleton often insert (Fig. 9D), better seen on images of the electrospinng scaffolds (DFN10e and DFN30e). Conversely, on casted scaffolds, few cells with stellate shaped and less developed actin cytoskeleton (Fig. 9D) were typically observed.

The morphology of the BMPC growing on the casted or fibrous scaffolds was observed by SEM (Fig. 10). It can be seen that cells attached and proliferate well on the film or fibrous scaffolds during 24 h of culture. In addition, it is possible to observe that the scaffolds keep their morphology unaltered during the rehearsal time. It was observed that more BMPC growth on the fibers scaffolds. These results agree with the morphological observations described in Fig. 9 and suggest that the topography and surface characteristic as well as the chemical nature of the scaffold may affect the development of these cells. We and other
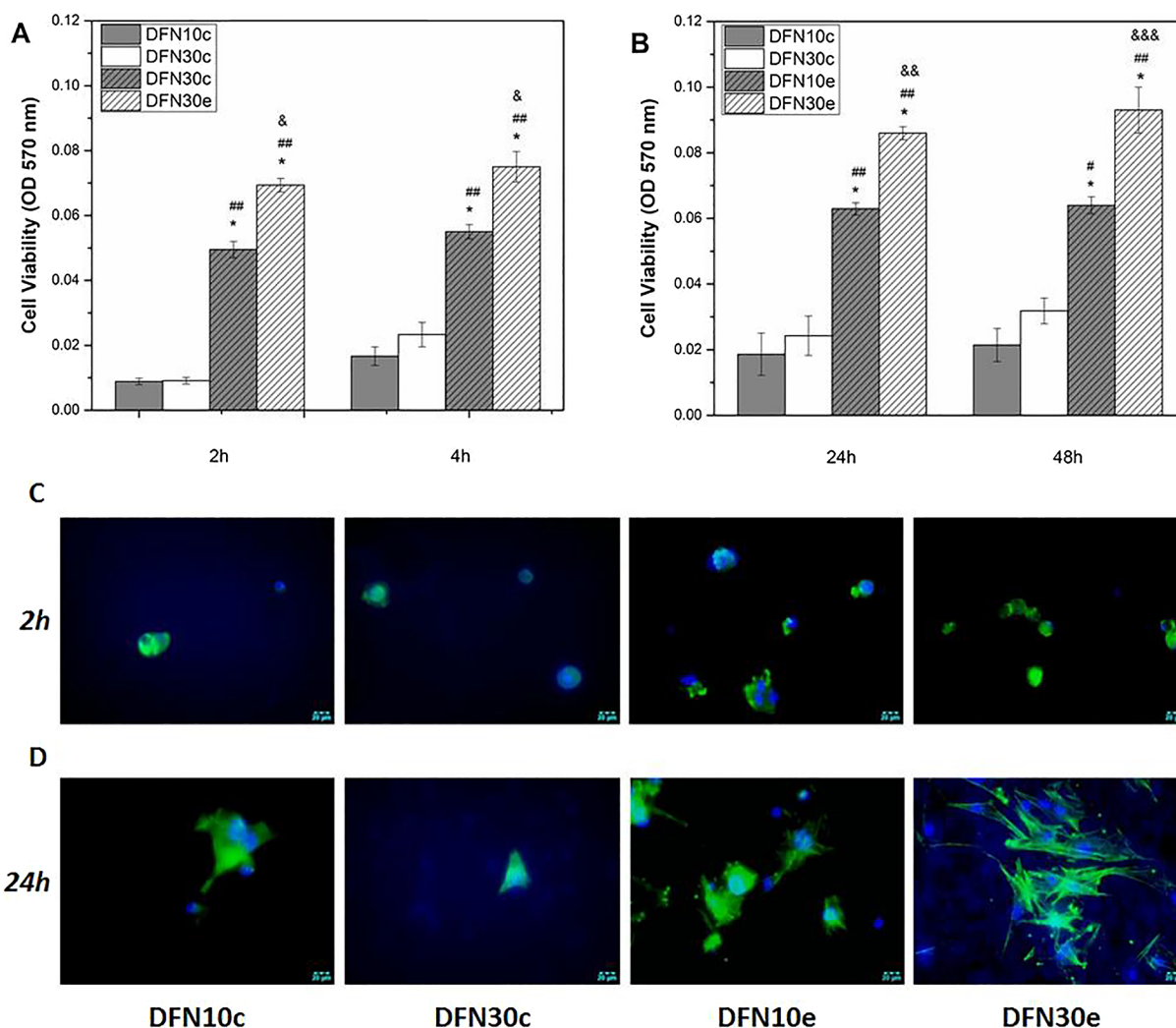
Fig. 9. Adhesion (2 and 4 h) and proliferation (24 and 48 h) of BMPC cultured on different scaffolds. Panel A and B represent the survival cells evaluated by MTT assay. Results represent the mean ± SEM, n = 8. Differences were: * $p < 0.001$ vs DFN10c; # $p < 0.05$, ## $p < 0.001$ vs DFN30c and & $p < 0.05$, && $p < 0.01$, &&& $p < 0.001$ DFN10e, for each culture period. Panel C and D show cells on different scaffolds after 2 h or 24 h, respectively. The actin fibers were stained with Alexa Fluor488 phalloidin (green) and the nucleus with Hoechst (blue). Obj. 40x. (For interpretation of the references to color in this figure legend, the reader is referred to the web version of this article.)

groups have previously demonstrated that this could be the case, since the attachment, spreading and growth of cells is modulated for clues that the surface is probably sending to the cells [11,31,40,41]. For instance, the interaction of integrins on cells membranes with the surface could induce biochemical signaling that in turn modulate cell growth and differentiation [29]. Thus, more investigation are needed in order to assessed the specific mechanism involves in these interactions.

It is known that the interaction of osteoblast with the matrix via integrins modulate their differentiation, function and survival [42]. These processes are regulated by several transcription factors that in turn lead to expression of different proteins involved in matrix production and mineralization. Osteoblast secreted type I collagen and other matrix protein to form the osteoid, over which the mineral hydroxyapatite will be deposited. ALP and osteocalcin are protein associated with these processes and represent markers for the osteoblast maturation during the osteoblastogenesis and bone formation. Runx2 and osterix are essential transcription factor for the osteoplastic differentiation, controlling the formation and remodeling of bone. Thus, several factors and signaling are involved in bone regeneration.

Due to our new biomaterials will be used for bone tissue regeneration, the osteoblastic differentiation on film or fibrous scaffolds were evaluated. For that matter, the ALP expression and the presence of

mineralized nodules were analyzed. Fig. 11 shows that ALP was expressed at low levels when cells grown in all scaffolds under a basal condition, suggesting that these materials or their topography do no induce any specific differentiation by itself. When cells were induced to differentiate in an osteogenic media, ALP increased significantly in the TCP-control condition and clear differences were observed between the scaffolds. Cells growing in the scaffolds prepared with highest DOF content (DFN30) expressed more ALP than in the corresponding basal media ($p < 0.001$ for DFN30c; $p < 0.05$ for DFN30e). Moreover, this stimulation was greater in a casted matrix (DFN30c) in comparison with the fibrous scaffolds (DFN30e).

In addition, the ability of BMPC to mineralize the matrix was assessed after 21 d in culture under basal or differentiation condition. Fig. 12 shows that cells expressed minimal mineralization in the presence of a basal condition, and no differences between the TCP or scaffolds were observed, in agreement with the results found for ALP expression. However, in the presence of an osteogenic media the calcium mineralization was statistically stimulated when cells grown on TCP or DFN10c, DFN30c or DFN30e ($p < 0.001$ vs basal). Nevertheless, cells mineralize better on the DFN30c matrix than on the other ones.

The osteogenic media-induced matrix mineralization seems to be similar to the ALP response (Fig. 11). Nevertheless, when cells grown
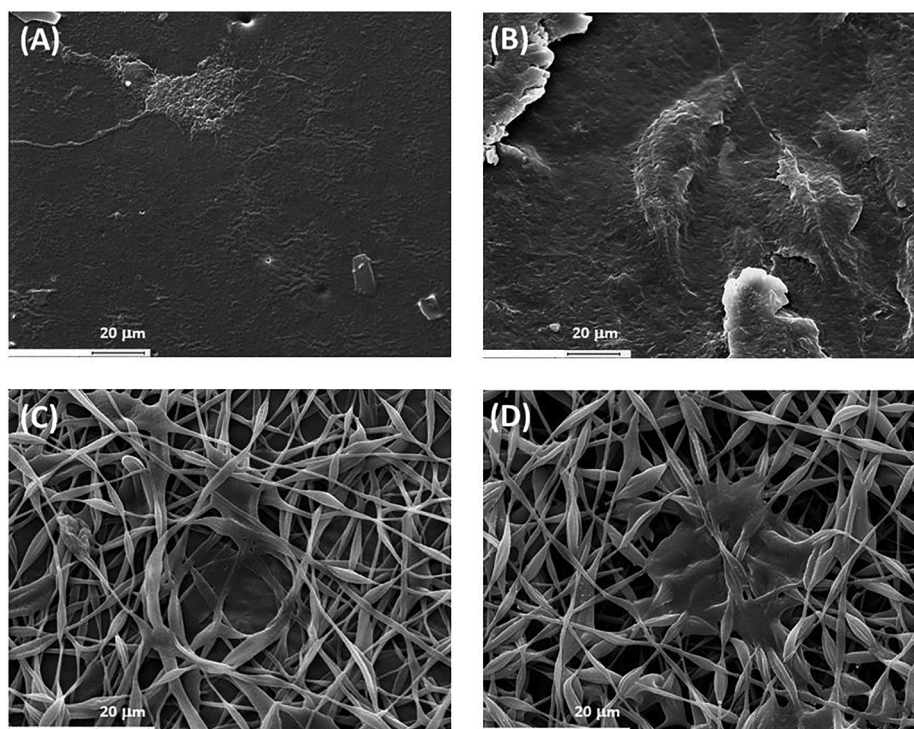
Fig. 10. SEM images of a BMPC growing on the surface of: (A) and (B) solution-cast films of DFN10c and DFN30c, respectively; (C) and (D) fibrous scaffolds formed by electrospinning of DFN10e and DFN30e, respectively. Time 24 h. Magnification 500X.
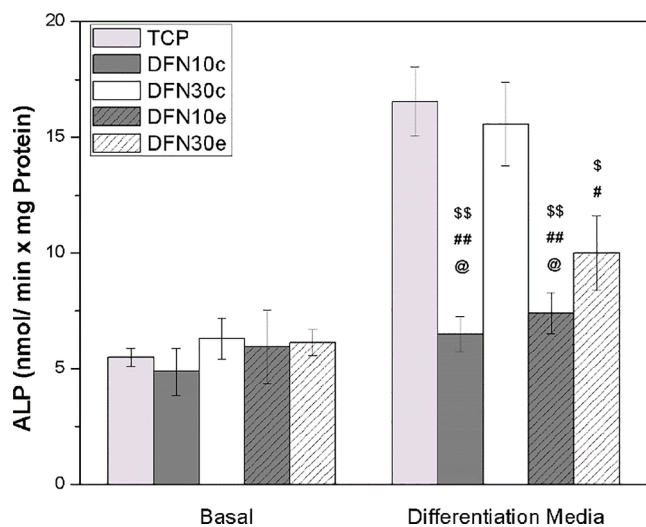

Fig. 11. Expression of ALP of BMPC growing on different scaffolds in a basal o differentiation media during 15 d of cultures. Results represent the mean ± SEM, n = 6. Differences were: $ $p < 0.01$; $$ $p < 0.001$ vs TCP, # $p < 0.05$; ## $p < 0.001$ vs DFN30c, @ $p < 0.05$ vs DFN30e.

Fig. 12. Production of nodules of mineralization by BMPC growing on different scaffolds in a basal o differentiation media during 21 d of cultures. Results represent the mean ± SEM, n = 10. Differences were: $p < 0.01$; $$ $p < 0.001$ vs TCP, # $p < 0.001$ vs DFN30c, *$p < 0.001$ vs DFN10c.

on DFN10c scaffolds cells produced mineralized nodules although not express more ALP than in the basal condition. These observations suggest that beside ALP other factors are still working on in the process of matrix mineralization. More studies are needed to clarify this process.

Altogether, the biocompatibility studies suggest that all scaffolds are good to promote the growth and differentiation of BMCP, although some differences were apparent. Comparatively, the differentiation of the cells is greater when they grow on the more hydrophobic scaffolds (DFN30). The results could be consequence of the biomaterial-cell interactions based on the chemical nature of the material that have highest DOF content. Similar results were previously reported [30].
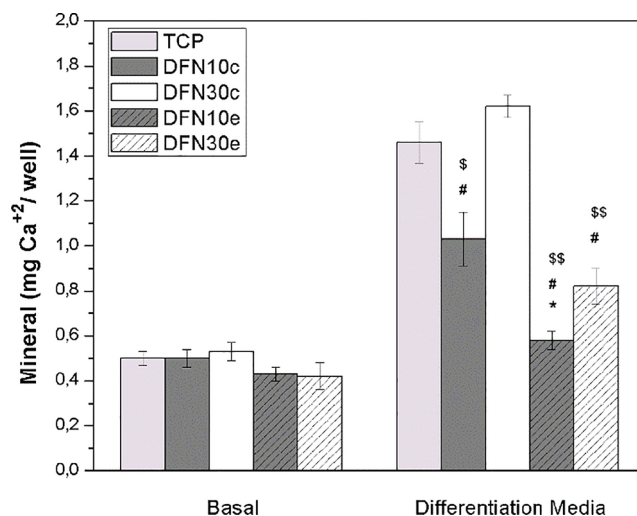
4. Conclusions

In this study new fumaric copolymers were synthesized starting to dioctyl fumarate (DOF) and N-isopropylacrylamide (NIPAM) using two azo initiator (AIBN and MAIB), which exhibited different initiation efficiency. Under the same experimental conditions, differences in composition and macromolecular characteristics were observed, depending of the initiator employed. All copolymers exhibited high thermal stability which makes them suitable to withstand thermal processing at temperatures up to 200 °C. Two copolymers were selected based on their properties for design scaffolds by casting or electrospinning methodologies. In the first case a smooth and homogeneous surface

morphology was observed, while microfibrous scaffolds were obtained in the second case. Both kind of scaffolds shows differences in water contact angle and degradation rate under cellular conditions (Raw 264.7 macrophages), demonstrating the effect of the structural characteristics as well as the surface morphology on their properties. Neither of them shows cytotoxic effect.

Studies of adhesion, proliferation and osteoblastic differentiation were carried out with BMPC cells. Greater cellular viability was found in the materials obtained by the electrospinning technique. Although all the scaffolds exhibit good osteogenic capacity, it was significantly increased on the scaffolds which have more fumaric content and more homogeneous surface (by casting technique). All our results suggest that the biomaterials obtained have excellent characteristics to be applied in bone tissue regeneration.

Declaration of Competing Interest

The authors declared that there is no conflict of interest.

Acknowledgments

References

[1] T. Ghassemi, A. Shahroodi, M.H. Ebrahimzadeh, A. Mousavian, J. Movaffagh, A. Moradi, Current concepts in scaffolding for bone tissue engineering, Arch. Bone Jt. Surg. 6 (2018) 90–99.

[2] G. Turnbull, J. Clarke, F. Picard, P. Riches, L. Jia, F. Han, B. Li, W. Shu, 3D bioactive composite scaffolds for bone tissue engineering, Bioact. Mater. 3 (2017) 278–314.

[3] T. Winkler, F.A. Sass, G.N. Duda, K. Schmidt-Bleek, A review of biomaterials in bone defect healing, remaining shortcomings and future opportunities for bone tissue engineering: the unsolved challenge, Bone Joint Res. 7 (2018) 232–243.

[4] Xiaoping Yang, Dongzhi Yang, Xiaolei Zhu, Jun Nie, Guiping Ma, Electrospun and photocrosslinked gelatin/dextran–maleic anhydride composite fibers for tissue engineering, Eur. Polym. J. 113 (2019) 142–147.

[5] B. Sultankulov, D. Berillo, K. Sultankulova, T. Tokay, A. Saparov, Progress in the development of chitosan-based biomaterials for tissue engineering and regenerative medicine, Biomolecules 9 (9) (2019) E470, https://doi.org/10.3390/biom9090470 Review.

[6] M. Abbasian, B. Massoumi, R.M. Rezaei, H. Samadian, M. Jaymand, Scaffolding polymeric biomaterials: are naturally occurring biological macromolecules more appropriate for tissue engineering? Int. J. Biol. Macromol. 134 (2019) 673–694.

[7] O. Janoušková, Synthetic polymer scaffolds for soft tissue engineering, Physiol. Res. 67 (Suppl 2) (2018) S335–S348.

[8] M.S. Cortizo, M.S. Molinuevo, A.M. Cortizo, Biocompatibility and biodegradation of polyesters and polyfumarates based-scaffold for bone tissue engineering, J. Tissue Eng. Regen. Med. 2 (2008) 33–42.

[9] J.M. Fernández, M.S. Molinuevo, A.D. McCarthy, A.M. Cortizo, M.S. Cortizo, Characterization of poly(ε-caprolactone)/Polyfumarate blends as scaffolds for bone tissue engineering, J. Biomat. Sci. Polym. Ed. 21 (2010) 1297–1312.

[10] J.M. Fernández, M.S. Cortizo, A.M. Cortizo, Fumarate/ceramic composite based scaffolds for tissue engineering: evaluation of hydrophylicity, degradability, toxicity and biocompatibility, J. Biomat. Tissue Eng. 4 (2014) 227–234.

[11] M.L. Lastra, M.S. Molinuevo, A.M. Cortizo, M.S. Cortizo, Fumarate copolymer – chitosan crosslinked scaffold directed to osteochondrogenic tissue engineering, Macromol. Biosci. 17 (2018) 1600219.

[12] M. Pasqualone, T.G. Oberti, H.A. Andreetta, M.S. Cortizo, Fumarate copolymers-based membranes overlooking future transdermal delivery devices: synthesis and properties, J. Mater. Sci. Mater. Med. 24 (2013) 1683–1692.

[13] M. Pasqualone, H.A. Andreetta, M.S. Cortizo, Risedronate transdermal delivery system based on a fumaric copolymer for therapy of osteoporosis, Mater. Sci. Eng. C Mater. Biol. Appl. 76 (2017) 652–658.

[14] S. Lanzalaco, E. Armelin, Poly(N-isopropylacrylamide) and copolymers: a review on recent progresses in biomedical applications, Gels 3 (2017) E36.

[15] G.A. Mortimer, A new high-temperature free-radical source, J. Org. Chem. 30 (1965) 1632–1634.

[16] M.L. Bravi Costantino, T.G. Oberti, A.M. Cortizo, M.S. Cortizo, Matrices based on lineal and star fumarate-metha/acrylate copolymers for bone tissue engineering: characterization and biocompatibility studies, J. Biomed. Mater. Res. A. 107 (2019) 195–203.

[17] M.S. Molinuevo, L. Schurman, A.D. McCarthy, A.M. Cortizo, M.J. Tolosa, M.V. Gangoiti, V. Arnol, C. Sedlinsky, Effect of metformin on bone marrow progenitor cell differentiation: in vivo and in vitro studies, J. Bone Miner. Res. 25 (2010) 211–221.

[18] Guidelines on Handling and Training of Laboratory Animals, Purl UFA ed, The Biological Council of Animal Research, Welfare Panel, Guide for the care and use of laboratory animals: Eighth Edition, The National Academies Press, Washington D.C, 2011.

[19] J.M. Fernandez, T.G. Oberti, L. Vikingsson, J.L. Gómez Ribelles, A.M. Cortizo, Biodegradable polyester networks including hydrophilic groups favor BMSCs differentiation and can be eroded by macrophage action, Polym. Deg. Stab. 130 (2016) 38–46.

[20] A.M. Cortizo, M.S. Molinuevo, D.A. Barrio, L. Bruzzone, Osteogenic activity of vanadyl(IV)-ascorbate complex: evaluation of its mechanism of action, Int. J. Biochem. Cell Biol. 38 (2006) 1171–1180.

[21] T. Otsu, A. Matsumoto, K. Shiraishi, N. Amaya, Y. Koinuma, Effect of the substituents on radical copolymerization of dialkyl fumarates with some vinyl monomers, J. Polym. Sci: Part A: Polym. Chem. 30 (1992) 1559–1565.

[22] T.G. Oberti, J.L. Alessandrini, M.S. Cortizo, Thermal characterization of novel p-nitrobenzylacrylate-diisopropyl fumarate copolymer synthesized under microwave energy, J. Therm. Anal. Calorim. 109 (2012) 1525–1531.

[23] A. Matsumoto, T. Sumihara, Thermal and mechanical properties of random copolymers of diisopropyl fumarate with 1-adamantyl and bornyl acrylates with high glass transition temperatures, J. Polym. Sci: Part A: Polym. Chem. 55 (2017) 288–296.

[24] M. Yoshioka, T. Otsu, Reactivity of primary radicals in the radical polymerization of dialkyl fumarates initiated with dimethyl 2,2'-azobis(isobutyrate) and 2,2'-azobis(isobutyronitrile), Macromolecules 25 (1992) 2599–2602.

[25] M.E. Silva, E.R. Dutra, V. Mano, Preparation and thermal study of polymers derived from acrylamide, Polym Deg Stab. 67 (2000) 491–495.

[26] T. Otsu, T. Yasuhara, A. Matsumoto, Synthesis, characterization and application of poly(substitued methylene)s, J. Macromol. Sci., Chem A 25 (1988) 537–554.

[27] D. Cochin, A. Laschewsky, N. Pantoustier, New substituted polymethylenes by free radical polymerization of bulky fumarates and their properties, Polymer 41 (2000) 3895–3903.

[28] S.D. Baruah, D. Sarmah, N.C. Laskar, Copolymers of bulky fumarate: synthesis and their properties, J. Polym. Res. 18 (2011) 225–233.

[29] M.J. Dalby, N. Gadegaard, R.O. Oreffo, Harnessing nanotopography and integrin-matrix interactions to influence stem cell fate, Nat Mater. 13 (2014) 558–569.

[30] M.L. Lastra, M.S. Molinuevo, J.M. Giussi, P.E. Allegretti, I. Blaszczyk-Lezak, C. Mijangos, M.S. Cortizo, Tautomerizable β-ketonitrile copolymers for bone tissue engineering: studies of biocompatibility and cytotoxicity, Mat. Sci. Eng. C 51 (2015) 256–262.

[31] S. Park, G.I. Im, Stem cell responses to nanotopography, J. Biomed. Mater. Res. A 103 (2015) 1238–1245.

[32] G. Ramírez, S.E. Rodil, H. Arzate, S. Muhl, J.J. Olaya, Niobium based coatings for dental implants, Appl. Surf. Sci. 257 (2011) 2555–2559.

[33] M. Simon, I. Behrens, L.A. Dailey, M. Wittmar, T. Kissel, Nanosized insulin-complexes based on biodegradable amine-modified graft polyesters poly[vinyl-3-(diethylamino)-propylcarbamate-co-(vinyl acetate)-co-(vinyl alcohol)]-graft-poly(l-lactic acid): Protection against enzymatic degradation, interaction with Caco-2 cell monolayers, peptide transport and cytotoxicity, Eur. J. Pharm. Biopharm. 66 (2007) 165–172.

[34] A.B.D. Cassie, S. Baxter, Wettability of porous surfaces, Trans. Faraday Soc. 40 (1944) 546–551.

[35] R.N. Wenzel, Resistance of solid surfaces to wetting by water, Ind. Eng. Chem. Res. 28 (1936) 988–994.

[36] M.P. Pavlov, J.F. Mano, N.M. Neves, R.L. Reis, Fibers and 3D mesh scaffolds from biodegradable starch-based blends: production and characterization, Macromol. Biosci. 4 (2004) 776–784.

[37] P.K. Szewczyk, D.P. Ura, S. Metwally, J. Knapczyk-Korczak, M. Gajek, M.M. Marzec, A. Bernasik, U. Stachewicz, Roughness and fiber fraction dominated wetting of electrospun fiber-based porous meshes, Polymers (Basel) 11 (2018) E34, https://doi.org/10.3390/polym1101003.

[38] S. Bose, M. Roy, A. Bandyopadhyay, Recent advances in bone tissue engineering scaffolds, Trends Biotechnol. 30 (2012) 546–554.

[39] X. Wang, W. Chu, Y. Zhuang, D. Shi, H. Tao, C. Jin, K. Dai, J. Zhao, Y. Gan, Bone mesenchymal stem cell-enriched β-tricalcium phosphate scaffold processed by the screen-enrich-combine circulating system promotes regeneration of diaphyseal bone non-union, Cell Transplantat. 28 (2019) 212–223.

[40] A.M. Cortizo, G. Ruderman, F.N. Mazzini, M.S. Molinuevo, I.G. Mogilner, Novel vanadium-loaded ordered collagen scaffold promotes osteochondral differentiation of bone marrow progenitor cells, Int. J. Biomater. 2016 (2016) 1486350.

[41] P. Tsimbouri, N. Gadegaard, K. Burgess, K. White, P. Reynolds, P. Herzyk, R. Oreffo, M.J. Dalby, Nanotopographical effects on mesenchymal stem cell morphology and phenotype, J. Cell Biochem. 115 (2014) 380–390.

[42] T. Bellido, L.I. Plotkin, A. Bruzzaniti, Bone cells, Basic and Applied Bone Biology, Elsevier Inc., 2013, pp. 27–45.